PROCEEDINGS OF SPIE

SPIEDigitalLibrary.org/conference-proceedings-of-spie

Using ellipsometry and x-ray photoelectron spectroscopy for real-time monitoring of the oxidation of aluminum mirrors protected by ultrathin MgF2 layers

Brian I. Johnson, Tahereh G. Avval, Grant T. Hodges, Victoria Carver, Karen Membreno, et al.

Brian I. Johnson, Tahereh G. Avval, Grant T. Hodges, Victoria Carver, Karen Membreno, David D. Allred, Matthew R. Linford, "Using ellipsometry and x-ray photoelectron spectroscopy for real-time monitoring of the oxidation of aluminum mirrors protected by ultrathin MgF2 layers," Proc. SPIE 11116, Astronomical Optics: Design, Manufacture, and Test of Space and Ground Systems II, 111160O (9 September 2019); doi: 10.1117/12.2529893

SPIE.

Event: SPIE Optical Engineering + Applications, 2019, San Diego, California, United States

Downloaded From: https://www.spiedigitallibrary.org/conference-proceedings-of-spie on 14 Sep 2019 Terms of Use: https://www.spiedigitallibrary.org/terms-of-use

Using ellipsometry and x-ray photoelectron spectroscopy for real-time monitoring of the oxidation of aluminum mirrors protected by ultrathin MgF_2 layers

Brian I. Johnson[a], Tahereh G. Avval[a], Grant T. Hodges[a], Victoria Carver [a], Karen Membreno[a], David D. Allred[b*], Matthew R. Linford[a]
[a]Department of Chemistry and Biochemistry, Brigham Young University, C100 BNSN, Provo, Utah USA 84602 [b]Department of Physics and Astronomy, Brigham Young University, N265 ESC, Provo, Utah USA 84602

ABSTRACT

To maintain high, broad-band reflectance, thin transparent fluoride layers, such as MgF_2, are used to protect the of aluminum mirrors against oxidation since aluminum oxide absorbs short wavelength light. In this study, we present, for the first time, combined X-ray photoelectron spectroscopy (XPS) and ellipsometric (SE) studies of aluminum oxidation as a function of MgF_2 over a range of layer thickness (0-6 nm). We also show for the first time, dynamic SE data which, with appropriate modeling, tracks the extent of oxide growth every few seconds over a period of several hours after the evaporated Al + MgF_2 bilayer is removed from the deposition chamber, exposing it to the air. For each SE data set, because the optical constants of ultrathin metals films depend strongly on deposition conditions and their thickness, the optical constants for Al, as well as the Al and Al_2O_3 thicknesses, were fit. SE trends were confirmed by X-ray photoelectron spectroscopy. There is a chemical shift in the Al 2s electron emission peak toward higher binding energy as the metal oxidizes to Al^{+3}. The extent of oxide growth can be modeled from the relative area of each peak once they are corrected for the attenuation through MgF_2 layer. This generates an empirical formula: oxide thickness= k*log(t) +b, for the time-dependent aluminum-oxide thickness on aluminum surfaces protected by MgF_2 as a function of MgF_2 layer thickness. Here, k is a factor which depends only on MgF_2 thickness, and decreases with increasing MgF_2 thickness. The techniques developed can illuminate other protected mirror systems.

Keywords: FUV, aluminum mirror coatings, oxidation, lifetime, XPS, spectroscopic ellipsometry, magnesium fluoride, quality assurance
*dda2@byu.edu; phone: 1+801-400-8277; fax 1 801 422-0553;

1. INTRODUCTION

Aluminum has unique properties and numerous applications.[1–3] It is generally considered to an easy metal to work with. It has a relatively low melting point, it is ductile yet strong enough to be used in structural applications, it is lightweight, it can be alloyed, and it is unmatched in its ability to reflect light over a wide energy range.[4,5] A drawback to aluminum is that its surface oxidizes quickly. Of course, a small amount of oxide is not a limitation for most of aluminum's applications. However, aluminum oxide, even when only a few nanometers thick, absorbs short wavelength light, which significantly limits aluminum's ability to act as a mirror for the shortest wavelengths, collecting light over the widest possible wavelength range.[6–10] Because of the importance of aluminum and aluminum oxide, these materials have previously been studied by various experimental and theoretical methods, including X-ray photoelectron spectroscopy (XPS) and spectroscopic ellipsometry (SE).[11–17]

A general strategy for preventing aluminum from oxidizing while preserving its optical properties is to coat it with a wide-band-gap material.[18–21] These types of barrier layers, e.g., MgF_2 and other fluorides, have been used for decades to protect

Astronomical Optics: Design, Manufacture, and Test of Space and Ground Systems II, edited by Tony B. Hull, Dae Wook Kim, Pascal Hallibert, Proc. of SPIE Vol. 11116, 111160O · © 2019 SPIE
CCC code: 0277-786X/19/$21 · doi: 10.1117/12.2529893

Downloaded From: https://www.spiedigitallibrary.org/conference-proceedings-of-spie on 14 Sep 2019
Terms of Use: https://www.spiedigitallibrary.org/terms-of-use

aluminum reflectors, including those in the Hubble Space Telescope.[5,6,18,21] Indeed, aluminum is currently being proposed as the primary reflector for future space missions such as the LUVOIR project, which could be a flagship NASA space observatory for the 2020s and 2030s.[22–24] However, in spite of the importance of protecting aluminum mirrors, we are not aware of any systematic XPS analysis of MgF_2-protected aluminum mirrors. Here we present such a study. We show that XPS can be used to follow aluminum oxidation under 0 to 6 nm thick MgF_2 layers, and that its oxidation rate depends on the thickness of the MgF_2 over it, i.e., thicker MgF_2 films result in slower Al oxidation. Furthermore, for the first time, we correlate the XPS data with dynamic and static SE data showing definitively that the dielectric that ellipsometry detects in aging samples is oxide.

This document follows recent, related proceedings papers on SE and XPS analysis of the oxidation of MgF_2-protected aluminum.[17,25,26] In this study, we discuss our preparation and study via real-time/dynamic SE and XPS of several samples of MgF_2 on Al. Both the Al and MgF_2 were deposited by thermal evaporation. The resulting optical stacks were analyzed in real-time with scans taken repeatedly over four hours followed by measurements over hundreds of hours for same samples. The optical constants of ultrathin metal films can vary greatly depending on thickness, morphology, and deposition conditions. Accordingly, the optical constants of with our deposition system of the approximate thickness used in our study were obtained from a multisample analysis (MSA) of aluminum films coated with thick MgF_2 layers and bare aluminum with its native oxide coating. Several models were investigated. A relatively simple model with two parameters (the thickness of the aluminum and aluminum oxide layers) was found suitable to model the four-hour, dynamic data obtained from each sample. As expected, thicker MgF_2 films led to slower oxidation of the underlying aluminum. A phenomenological, parametric model of the oxidation kinetics with fluoride thickness is presented. Details follow herein.

2. EXPERIMENTAL

2.1 Deposition of Al and MgF_2 Bilayers

Aluminum + MgF_2 bilayer films were deposited using a Denton DV-502A thermal evaporator to study Al oxidation. The Al and the MgF_2 were deposited sequentially, without breaking vacuum between the Al and the MgF_2. This was done in a Denton (model DV-502 A) evaporator with two independent, resistance-heated evaporation sources. The evaporator also had a rotating sample stage to improve deposition thickness uniformity, an Inficon quartz-crystal thickness monitor (QCM) and a shutter activated by the thickness monitor to precisely control thicknesses. The over-night base pressure of the system was in the high 10^{-7} torr range. Aluminum was evaporated from a 1" piece of aluminum wire Al wire placed within a tungsten coil. The magnesium fluoride (99.99% ChemSavers) grains (total about 1.5 gm) were placed in a standard (RD Mathis) molybdenum evaporation boat.

Prior to deposition, the samples were cleaved from a 200-mm-diameter Si (100) wafer coated with a nominal 300 nm of CVD Si_3N_4. The CVD Si_3N_4 dielectric layer on the substrate is referred to as the interference layer (IL). The cleaved wafer pieces were mounted on the rotation stage and the system was pumped to a pressure in the low to mid 10^{-6} torr range. During deposition, the system pressure was observed to rise to ~$1.5x10^{-5}$ torr. This is thought to be due to water vapor's release in the chamber, as the walls are radiatively heated by the hot evaporation sources. The Al was deposited at a rate of 35 Å/sec to achieve a thickness of 150 Å. The MgF_2 was then immediately deposited (time between depositions was less than 60 seconds) on the Al film at a rate of 3 Å/sec. The time for both depositions was 35 to 45 s.

The time between the end of the evaporation of the aluminum film and the beginning of the evaporation of the overcoat was minimized to avoid oxide build up on the freshly evaporated Al and was usually less than 60 seconds. The voltage was set to be as high as practical to get evaporation rate of the l: 4-10 nm/sec. Past work has shown that high rates are conducive for producing the purest (highly reflective) aluminum layers. The high rates limit the incorporation of oxygen into the film.

It was not our goal to replicate state-of-the-art, front-surface aluminum mirrors in every detail. Rather, we aimed at producing materials and structures that facilitated SE study, but are otherwise as similar as possible to the relevant aspects of the best mirrors. Our films are test samples for answering scientific/technological questions, such as, "What is the rate of oxidation of aluminum coatings protected by a certain thickness of barrier?" We hypothesize that small amounts of oxygen incorporation are not likely to change oxidation rates significantly, though this should be investigated. Likewise, aluminum thickness might not affect aluminum oxidation rate. Thus, the behavior of our ultrathin aluminum coatings should be useful in understanding state-of-art aluminum mirrors.

Downloaded From: https://www.spiedigitallibrary.org/conference-proceedings-of-spie on 14 Sep 2019
Terms of Use: https://www.spiedigitallibrary.org/terms-of-use

Immediately following the depositions of Al and MgF_2, the chamber was vented with N_2, which took 1.5 –2 min. The samples were then removed and rushed to the SE and XPS for instruments. Removal from the deposition chamber marked the starting time for measuring sample aging for SE or XPS interpretation. At this point, each sample was divided into multiple pieces: one piece for SE analysis and the others for XPS.

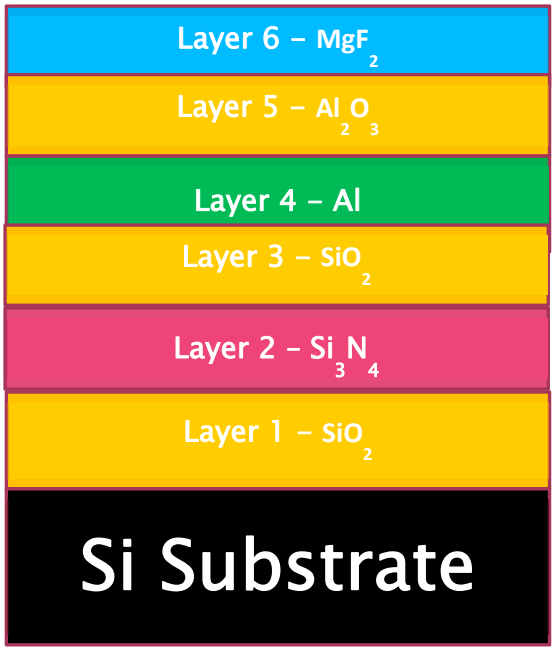


Figure 1. Representation of the optical stacks prepared and analyzed in this work. The bottom layers up through Layer 3 represent the Si/Si_3N_4 substrate. Layers 4 and 6 represent the Al and Mg deposited on the substrate. Layer 5 represents the oxidized Al that forms on the Al layer. Prior work had shown that the oxide does not form under the Al[17]

2.2 Ellipsometric characterization

Ellipsometric data was acquired using a J.A. Woollam M-2000D, variable-angle, spectroscopic ellipsometer (J.A. Woollam Company, Lincoln, ME, USA) over the wavelength range of 190-1688 nm. Time-dependent SE measurements were obtained for various samples using the 'in situ' mode of the instrument. The ellipsometer acquired delta and psi data at 75° every 2.3 s for a period of 4 h. Data were subsequently modeled using the CompleteEASE® SE instrument analysis software. The model in Figure 1 shows the types of stacks prepared and studied in this work. The optical constants for all layers except #2 and 4 were modeled with the optical constants in the CompleteEASE® data base, specifically these were: Si-JAW, SiO2 JAW (silicon native oxide) Layer 1 and 3, Layer 5-Al_2O_3 (parametric model) and Layer 6-MgF_2 (a Sellmeier model of the ordinary-ray refractive indices of MgF_2). The optical constants for 'Layer 2 CVD Si_3N_3' were obtained by measuring a number of substrates prior to deposition.[17] We found that the optical constants of silicon nitride could be parameterized successfully as a Tauc-Lorentz oscillator plus a Gaussian oscillator located near the band edge. Measurement were made on each specific sample prior to the deposition of the aluminum and fluoride. The Si_3N_4 thickness was then fit. On occasion, the thickness of this layer was sometimes fit to decrease the MSE of the substrate fit. These parameters were then held fixed during the analysis of the delta and psi data to get Al (Layer 4) and Al_2O_3 (Layer 5) thickness.

The optical constants for the aluminum film were obtained from multisample analyses as described in results. Interference enhancement, as the technique is known, has been found to increase significantly the sensitivity to the absorber optical properties and thickness. The purpose of a thick dielectric layer between the aluminum layer and the Si substrate is to enhance the information content of multiple-angle measurements.[17] Spectroscopic ellipsometry and transmitted or reflected intensity was shown, for example, to produce a unique result for the Cr films on fused silica substrates.[27] It should be noted that the Al in the films suitable for these ellipsometric studies are a factor of 3-4 times too thin for standard telescope mirrors.

Downloaded From: https://www.spiedigitallibrary.org/conference-proceedings-of-spie on 14 Sep 2019
Terms of Use: https://www.spiedigitallibrary.org/terms-of-use

2.3 XPS characterization

XPS was performed with a Surface Science SSX-100 instrument (maintained by Service Physics, Bend, OR, USA) with a hemispherical analyzer. The instrument employs monochromatic Al Kα X-rays. Survey scans were collected with an X-ray spot size of 800 x 800 μm^2 with a resolution of 4, nominal pass energy of 150 eV, 6 passes/scans, and a step size of 1 eV. High resolution scans were collected over the Al 2s region, centered at a binding energy of 120 eV, with an energy window of 40 eV and a step size of 0.0625 eV. The number of scans ranged between 15 and 35, and the spot size was 800 x 800 μm^2 with a resolution of 3 (nominal pass energy of 100 eV). Area ratios were calculated using the CasaXPS modelling software (Casa Software Ltd., Version 2.3.18PR1.0).

2.4 MgF_2 thickness standard preparation

MgF_2 thickness standards for XPS analysis allow the thickness of MgF_2 on Al films to be measured via XPS. To prepare the standards, MgF_2 films of four different thicknesses on Si were deposited on approximately 25 mm x 25 silicon pieces cleaved from a single-side polished 150 mm diameter epi silicon wafer. The samples had been cleaned by a low-pressure air plasma (Herrick). The native oxide thickness on each sample was then measured via ellipsometry prior to MgF_2 deposition. The native oxide thickness was about 1.5nm after the fluoride deposition, the thicknesses of the MgF_2 layers were also measured via SE at an angle of 75°. Modeling was performed using the optical functions in the instrument software for MgF_2 (MgF_2 (Sellmeier)) and Si/SiO_2 (Si_JAW and SIO2_JAW, respectively) to obtain the fluoride thickness. After this, the pieces were analyzed with XPS. This included narrow scans of the Mg 2s and Al 2p features.

3. RESULTS AND DISCUSSION

3.1 Determination of fluoride thickness

In spectroscopic ellipsometry (SE), light of a known polarization state is directed onto a surface, and changes in that polarization are detected. Through creation of models and adjustment of the parameters in them, SE can be used to determine a variety of material properties including film thicknesses, surface roughness, and optical constants of materials. However, due to the complexity of the optical stack in the present work (see Figure 1), as noted elsewhere,[15, 25] the thickness of the MgF_2 layer could not be uniquely determined using spectroscopic ellipsometry due correlation with the potential aluminum oxide layer. While the thickness monitor provided thickness control, an independent measurement of the thickness of the deposited MgF_2 layer was desired.

We found that we could use XPS in conjunction with SE to make these measurements. In this analysis, we employed an equation from Cumpson, which is based on Hill's equation.[28,29] It is as follows:

$$ln\ \frac{(I_o/s_o)}{(I_s/s_s)} - \left[\left(\frac{E_o}{E_S}\right)^{0.75} - \frac{1}{2}\right]\frac{t}{\lambda_o\ cos\ cos\ \theta} - ln2 = ln\ sinh\ \left(\frac{t}{\lambda_o\ cos\ cos\ \theta}\right) \quad (1)$$

Here, I_o and s_o are the intensity and sensitivity factor respectively of the Mg 2s photoelectrons in the top layer of the MgF_2 standards (here, the MgF_2 film), and I_s and s_s are the intensity and sensitivity factor of the Si 2p electrons from the substrate (here, the Si/SiO_2 layer), and the take-off angle (cos θ in Equation 1) of our XPS system is 35°. Finally, ellipsometric thicknesses for MgF_2 films on the silicon standards were used for thickness (here, t) in Equation 1 as well. Equation 1 was first used to assess the attenuation coefficient, λ_o, for MgF_2 using the MgF_2 standards evaporated on Si substrates described in section 2.4. Peak areas (I_o and I_s here) and binding energies (E_o and E_s for Mg 2s and Si/SiO_2 2p photoelectrons, respectively) were calculated. Iterations of λ_o were performed until both sides were of equal value. This resulted in four different values of λ_o: (1.6 nm MgF_2, λ_o: 6.1 nm), (2.1 nm MgF_2, λ_o: 5.3 nm), (3.3 nm MgF_2, λ_o: 4.6 nm), and (5.1 nm MgF_2, λ_o: 4.2 nm). These results showed a decreasing trend in the attenuation coefficient as MgF_2 thickness increased. This is not particularly surprising, since the substrates were not heated while the MgF_2 was deposited. It is commonly seen that thin dielectric films are not fully dense when deposited on unheated surfaces, particularly the thinnest films. Porous films logically would have larger attenuation lengths. Because our studies covered MgF_2 thicknesses of ca 2 nm or greater, we used λ_o of 4.5nm in the proceeding steps.

Equation 1 can also be used to determine the thickness of the MgF_2 layer deposited on aluminum. Here, instead of Si/SiO_2 2p electrons for the substrate, Al 2p electrons were used for the substrate (here, the Al/Al_2O_3 layer). E_o and E_s are the

Downloaded From: https://www.spiedigitallibrary.org/conference-proceedings-of-spie on 14 Sep 2019
Terms of Use: https://www.spiedigitallibrary.org/terms-of-use

binding energies of Mg 2s and Al 2p photoelectrons respectively and λ_o is the attenuation coefficient of the aforementioned Mg 2s photoelectrons. These results were within 5% of the QCM value used to control the MgF_2 deposition thicknesses in the evaporator. Overall, this approach accounted for any run-to-run variation in the deposition of the MgF_2.

3.2 SE analysis

To study the oxidation of MgF_2 under aluminum, as described in section 2.1 Al (nominal thickness of 15 nm) and then MgF_2 (different thicknesses) were deposited onto fully characterized $Si/SiO_2/Si_3N_4/SiO_2$ substrates. These $Si/SiO_2/Si_3N_4/SiO_2/Al/MgF_2$ stacks were then removed from the evaporation chamber, which "started the clock" for the sample. As quickly as possible, each sample was moved to the ellipsometer, and a four-hour run was commenced that repeatedly collected SE data from the sample. The stack was then analyzed by XPS to determine the thickness of its MgF_2 layer.

The next step was to analyze the delta and phi ellipsometric data to obtain the time-dependent thickness of the oxide for each four-hour set of SE data. The key question is always- how can one employ the minimum number of fit parameters? Two approaches were explored. In the first approach (Model 1) only two unknowns were fit, the thickness of the aluminum oxide and the aluminum (see again Figure 1). This, as we discuss below, showed the correct trends but wrong thicknesses. In the second approach (Model 2), in addition to the two thicknesses, the aluminum optical constants were also fit for each sample. In both cases the SE models relied on determining and fixing as constants as many of the other layer thicknesses and optical constants as possible prior to depositing the $Al+MgF_2$ bilayers. These were: (i) the $Si/SiO_2/Si_3N_4/SiO_2$ substrate thicknesses and optical constants, (ii) the optical constants of Al_2O_3 that were in the instrument software, (iii) the thickness of MgF_2, that had been determined by XPS, and (iv) the optical constants of MgF_2 from the instrument software.

For Model 1, the same optical constants of Al were used for all samples. The optical constants of thin metal films depend strongly on their structure and deposition conditions, however.[27,30] Indeed, as Thompkins et al point out in dealing with metals, "with only a few exceptions, one must determine the optical constants …, and that it is inappropriate to use values from another source such as a handbook or from another investigator."[31] Thus, it was necessary to determine the optical constants of the Al films produced with our evaporation system. The instrument software was deemed an appropriate starting point, however. These constants were generated from 4 samples, each with the about the same Al thickness (15 nm) using a "multisample analysis" (MSA) in CompleteEase. The samples were (i) three Al films (nominally 15 nm thick) that were covered with thick films of MgF_2 (nominally 25 nm thick) and (ii) one bare aluminum surface (nominally 15 nm thick). As with similar bilayers, these layers were deposited onto silicon nitride ($Si/SiO_2/Si_3N_4/SiO_2$) substrates. Because

Table 1 Results from the two models used to analyze the dynamic sets of SE data generated in this study.

MgF_2 Thickness	**Model 1 MSE**	**Model 2 MSE**
0.000 nm	1.200	0.315
1.726 nm	0.754	0.410
2.096 nm	15.491	1.385
2.847 nm	3.275	2.930
3.550 nm	300.000	7.623
3.554 nm	1.234	0.370
4.322 nm	0.754	0.315
4.544 nm	16.961	3.515
5.358 nm	0.833	0.252
5.974 nm	33.685	5.813
Samples w/neg. Al_2O_3 thicknesses	6 of 9	2 of 10
Samples that could not be fit	1	0

Downloaded From: https://www.spiedigitallibrary.org/conference-proceedings-of-spie on 14 Sep 2019
Terms of Use: https://www.spiedigitallibrary.org/terms-of-use

of the thickness of the MgF_2 layers here, it was assumed that no aluminum oxide form under them after they were deposited. Though some oxide could form even in vacuum in the minute between the end of the Al deposition and the beginning of the fluoride deposition, it was assumed to be negligible compared to the MgF_2 thickness. Thus, the MgF_2 thickness was determined directly by SE. The bare aluminum film, on the other hand, was expected to have surface oxide, i.e., it was modeled as an aluminum layer beneath an Al_2O_3 layer. For this modeling, the optical constants of Al_2O_3 from the instrument software were used. The starting point for the optical constants of Al in the MSA was the "Al (Lorentz).mat" model in our instrument software, which contains seven Lorentzian oscillators. Each has three parameters. To determine the optical constants for our evaporated aluminum, the amplitudes and breadths, but not the positions, of these Lorentzians were allowed to vary one at a time. Epsilon naught, the dielectric constant at zero energy, was also fit. In this analysis, the amplitude of one of the Lorentzians went to zero so it was omitted from our Al model. The lowest energy Lorentzian was at an energy of 0 eV. It models the effect on optical constants of the free electrons. These are particularly influenced by grain-size and other structural effects. As in all analyses, prior to the deposition of Al and MgF_2, the thicknesses of the layers in the substrate (from the 'Si Substrate' through 'Layer 3 – SiO_2' layer) had been measured, modeled, determined, and then fixed.

Each model was applied to each set of dynamic data collected in each four-hour analysis from 10 different bilayer samples. The results are summarized in Table 1. The first column shows the thicknesses of the MgF_2 layer. The middle and last

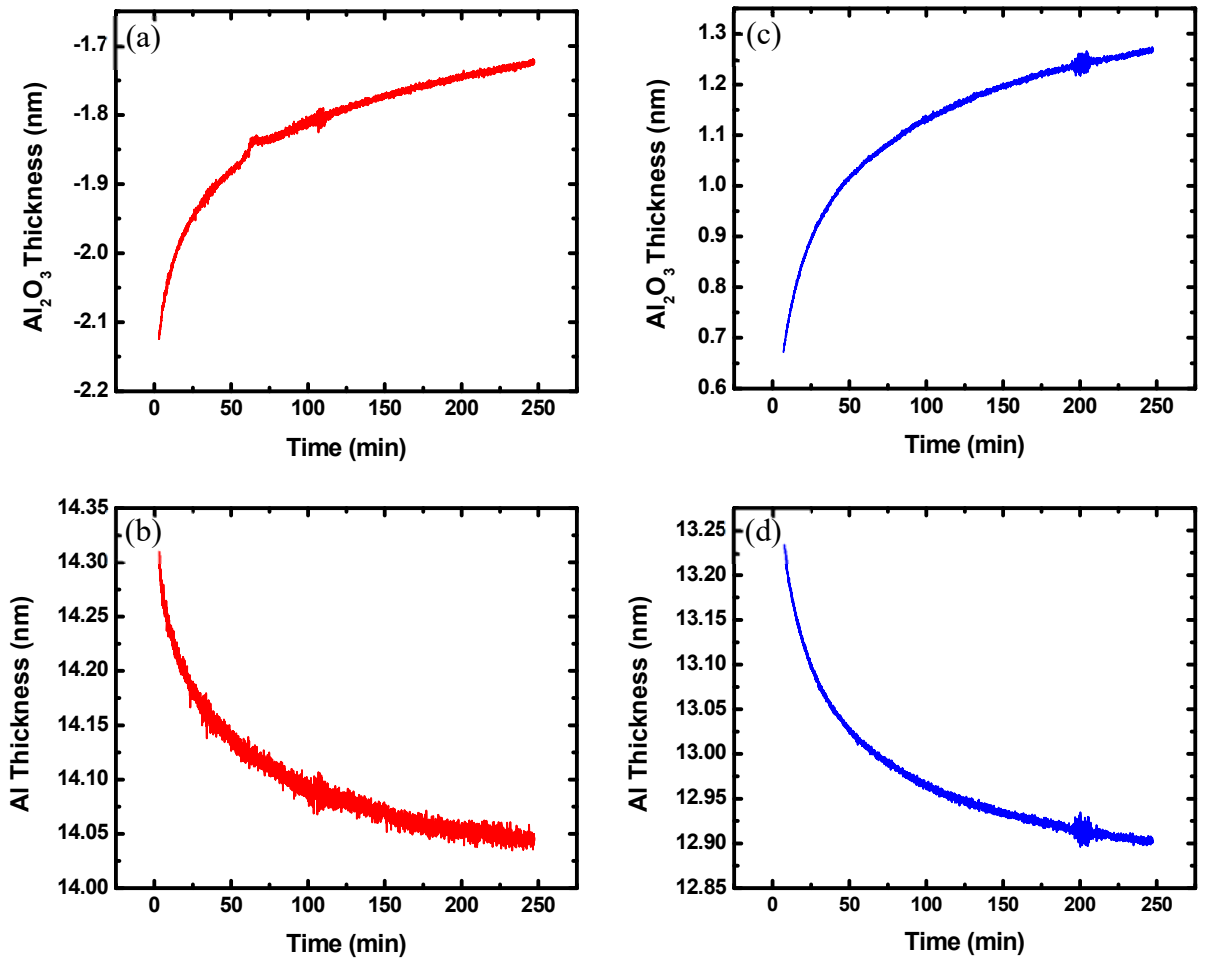


Figure 2. Thicknesses of Al_2O_3 and Al determined by Model 1 from two representative samples that showed negative (a) and positive (c) Al_2O_3 thicknesses. Also shown are the Al thicknesses obtained as a function of time for these surfaces.

Downloaded From: https://www.spiedigitallibrary.org/conference-proceedings-of-spie on 14 Sep 2019
Terms of Use: https://www.spiedigitallibrary.org/terms-of-use

column of Table 1 presents the mean squared error (MSE) value of the fits obtained with Model 1 and 2 respectively for each of these samples.

It is clear here that for the two thickness fit (Model 1) that while some of the data sets are well fit (lower MSE values), others are poorly fit (higher MSE values). The bottom rows of Table 1 report that with Model 1, one of the samples could not be fit (the one with an MSE of 300), and 6 of the remaining 9 samples showed at least some Al_2O_3 thicknesses that were negative. A negative thickness is obviously unphysical. Indeed, Figure 2 shows representative results from Model 1 for two samples with different MgF_2 thicknesses that gave positive and negative thicknesses for the Al_2O_3 layer. However, in spite of the fact that Model 1 predicted negative Al_2O_3 thicknesses for a significant fraction of the samples, all of the plots of Al_2O_3 and Al thicknesses for the samples that could be fit, showed the same trends. That is, there is increasing Al_2O_3 thicknesses and decreasing Al thicknesses with time. In particular, it was found that the plots of the Al_2O_3 thicknesses vs. time for the different samples were approximately straight lines, and that they could be reasonably fit to equation of the form:

$$d_{Al2O3} = k \ln t + b, \tag{2}$$

where d_{Al2O3} is the thickness of the Al_2O_3 film, t is time, k is a prefactor which describes how fast the sample oxidizes, and b is the y-intercept of the line. Figure 3 shows the values of k that were thus obtained are a function of MgF_2 thickness.

The negative thicknesses for Al_2O_3 predicted by Model 1 are somewhat disconcerting. We reasoned that perhaps this model was giving unphysical results for this layer because we were requiring the same optical constants for Al to be applied to all the stacks – we previously noted that optical constants for extremely thin metal films are *not* constant[15]. Accordingly, a second SE model/approach (Model 2) was developed in which the optical constants of Al were determined/allowed to vary for each sample (the amplitudes and breadths, but not the center energies, of all the Lorentzians varied). However, once a sample's Al layer optical constants were determined, those same constants are used throughout the time sequence for analyzing thicknesses. The lower MSE values for Model 2 (see Table 1) suggested that this approach more closely represented each material. In other words, the improved MSE values support the idea that the Al optical constants vary between the samples. Two other indications that Model 2 is an improved representation of our materials are that all of the samples could be fit with Model 2, and only 2 of the 10 samples showed "negative Al_2O_3 thicknesses". Plots of Al_2O_3 thickness vs. the log of time were again found to be quite linear and were fit with Equation 2.

The resulting k values are plotted in Figure 3. It is significant that they are nearly identical to those obtained with Model 1. That is, these results suggest that the decrease in k observed with increasing MgF_2 thickness is not an artifact of either approach to measurement samples. It is clear that k decreases as the thickness of the MgF_2 over layer increases, which is the expected behavior for this system. Figure 3 shows that the values of k that were thus obtained as a function of the MgF_2

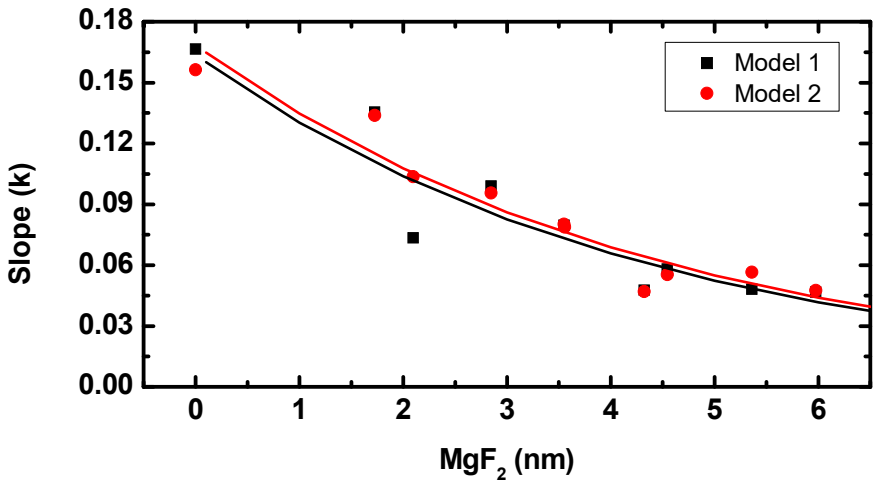


Figure 3. Values of k determined from Equation 1 from data generated from Models 1 and 2 employed in this study.

Downloaded From: https://www.spiedigitallibrary.org/conference-proceedings-of-spie on 14 Sep 2019
Terms of Use: https://www.spiedigitallibrary.org/terms-of-use

thickness are not an artifact of the model but point to underlying behavior. That is, these results suggest that the decrease in k observed with increasing MgF_2 thickness is not an artifact of either measurement samples.

3.3 X-ray Photoelectron Spectroscopy Analysis

As we noted previously, the thickness of the MgF_2 layer on Al could not be modeled unequivocally using SE due potential correlation with the Al_2O_3 layer. Therefore, to measure the thickness of the MgF_2 layer, XPS itself was used in conjunction with SE. XPS is a surface sensitive technique that probes ca. 10 nm into a surface. It can monitor elemental compositions and oxidation states of materials as well. XPS data are modelled using curve fitting techniques that account for differences in composition. This peak fitting is important because XPS line widths and chemical shifts due to changes in oxidation states are of comparable size.[32] To study the oxidation rates of Al as a function of MgF_2 thickness, as discussed in section 2.4, four silicon pieces had Al deposited onto them along with various thicknesses of MgF_2 in an in-situ deposition. All samples were analyzed at the Al 2s binding energy (BE) position of 118 eV. We chose the Al 2s region for data collection over the Al 2p region because the intensities were very similar, but with Al 2s, we did not have to consider spin-orbit splitting as is seen in Al 2p peak analysis. For Al 2s peak fitting, two types of synthetic line shapes were considered: Gaussian Lorentzian product (GLP) functions, and Gaussian Lorentzian sum (GLS) functions.[33]

For our analyses, we used GLS because it fit our data better than the GLP functions. The shape characteristics of Al metal exhibited stronger Lorentzian characteristics than that of Al_2O_3.[33,34] This is due to the disorder in the oxide and phonon broadening in it.[16,35,36] The Lorentzian characteristic value determination in GLS for the Al_2O_3 and Al was done by varying the percent Lorentzian characteristic of the peaks and using the standard deviation of the residuals (STDEVRes) between the peak fit and raw data over all of the samples analyzed. A lower STDRes value shows less discrepancy between peak models and the actual data and therefore a better fit. However, in our data, because both sets of peaks (Al_2O_3 and Al) are

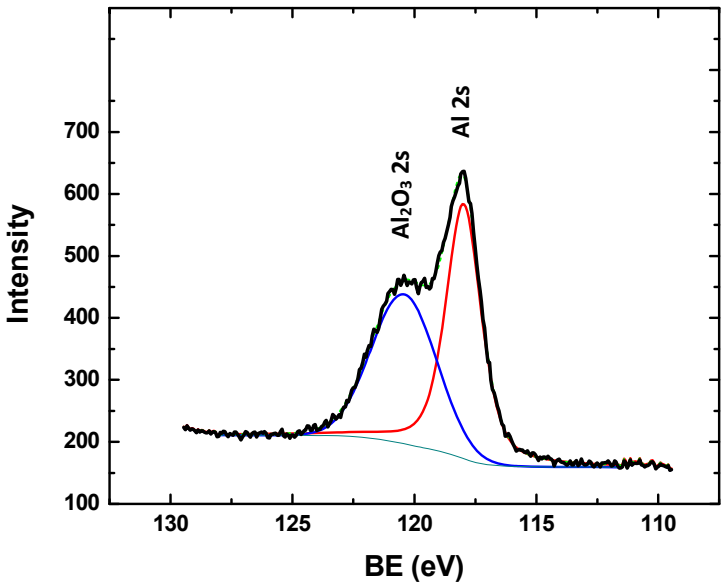


Figure 4 Al_2O_3 and Al peaks under same peak envelope

under the same general peak envelope as shown in Figure 4, the Lorentzian and Gaussian operators will interact with each other and can affect the STDRes. Therefore, to make the STDRes work as a figure of merit, the Lorentzian characteristics for both Al_2O_3 and Al were varied with each other and the resulting associated STDRes values were plotted against each other in Figure 5 From these results, the GLS values of 50 for Al and 0 for Al_2O_3 were chosen as the shapes for peak fitting the data. Using these parameters, we were able to quantify the areas under the individual Al_2O_3 and Al peaks with a high degree of confidence.

Downloaded From: https://www.spiedigitallibrary.org/conference-proceedings-of-spie on 14 Sep 2019
Terms of Use: https://www.spiedigitallibrary.org/terms-of-use

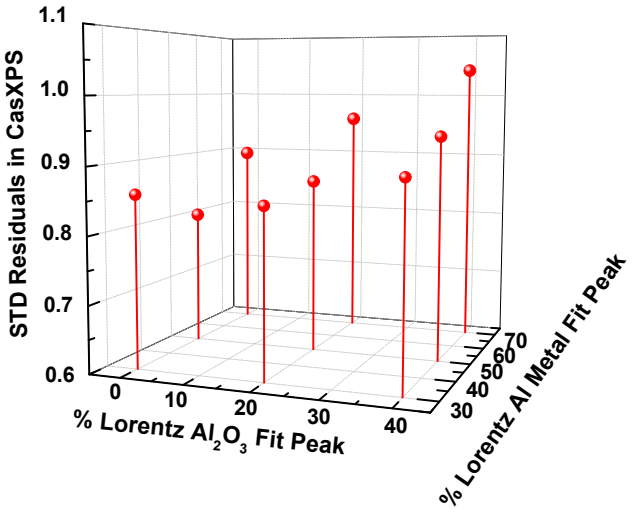


Figure 5 Values of k determined by Equation 2 from XPS peak data fit using GLS values of 50 for Al and 0 for Al_2O_3.

Oxidation rate studies of the Al samples were completed by monitoring the change of Al_2O_3/Al ratios over time. Figure 6 presents a visual display how the Al is oxidized into Al_2O_3 over time. By calculating the area under each curve and then comparing them, changes in the Al_2O_3/Al ratios were able to be quantified and rates were able to be gathered. Our data showed the average full width half maximum (FWHM) for the Al and Al_2O_3 2s peaks to be 1.72 ± 0.07 eV and 2.98 ± 0.13 eV respectively. The oxide peak FWHM values were within 10% of literature γ-Al_2O_3 values and the Al metal peaks were within 15% of literature values.[32,35–37] In addition, average binding energy (BE) differences between Al_2O_3 and Al peaks were 2.57 ± 0.12 eV with an average FWHM ratio of 1.73 ± 0.09 eV. These results are tabulated in Table 2. The consistency of the statistics in Table 2 also increased our confidence in the validity of our data. Using these standards, we were able to quantify aluminum oxidation changes over time. As such, we can show the graphical representation of changes in the aluminum oxidation starting from immediate removal from the evaporator chamber and extending to 8 months. In Figure 7, Al_2O_3/Al ratios are graphed as functions of the log of time. It can be observed that plotting the data points as a function of the log of time shows points fall, more or less, on a straight line. Empirically, then, oxidation followed a logarithmic model over an extended time-period of observation. That the rate of oxidation decreases with time is not surprising since as the oxide film thickness grows, it creates a protective boundary that greatly reduces atmospheric oxygen or water access to the aluminum metal surface.[17]. As shown, the rates were empirically fit using regression analysis to the general equation using the Al_2O_3 to Al ratios shown in Equation 3:

$$Al_2O_3/Al = k \ln t + b \quad (3)$$

Here k is the slope. Table 3 gives changes in oxidation prefactors as a function of the MgF_2 thicknesses

Table 2 Statistics for Al 2s Peaks

MgF_2 Thickness (nm)	**Average FWHM Al 2s Peak**	**Average FWHM Al_2O_3 2s Peak**	**Average BE Difference Al/Al_2O_3 2s Peaks**	**Average FWHM Ratio Al_2O_3 /Al 2s Peaks**
1.82	1.76 +/- 0.14	2.96 +/- 0.14	2.49 +/- 0.1	1.68 +/- 0.09
2.20	1.68 +/- 0.06	2.82 +/- 0.08	2.59 +/- 0.08	1.68 +/- 0.08
2.30	1.74 +/- 0.04	2.99 +/- 0.08	2.46 +/- 0.04	1.72 +/- 0.06
3.08	1.71 +/- 0.04	3.15 +/- 0.22	2.75 +/- 0.24	1.84 +/- 0.16
Average	**1.72 +/- 0.07**	**2.98 +/- 0.13**	**2.57 +/- 0.12**	**1.73 +/- 0.09**

Downloaded From: https://www.spiedigitallibrary.org/conference-proceedings-of-spie on 14 Sep 2019
Terms of Use: https://www.spiedigitallibrary.org/terms-of-use

Table 3 Oxidation rate prefactors from different MF_2 thicknesses

MgF_2 Thickness	**$y = k \ln t + b$ k**
1.818	0.064
2.196	0.041
2.302	0.043
3.077	0.035

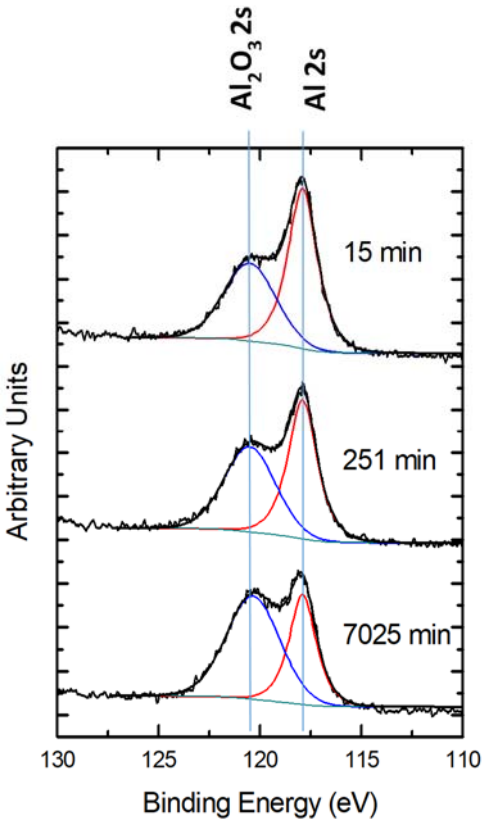


Figure 6: XPS spectra of Al_2O_3 & Al over time.

4. CONCLUSIONS

Recent ellipsometric studies showed changes in aluminum films under ultrathin films of magnesium or aluminum fluoride that could be interpreted as oxidation of the aluminum forming an oxide layer on top, but this interpretation was not proved. Here, XPS measurements shows that indeed in the case of MgF_2 films with thicknesses between 0-6 nm these changes are due to the slow oxidation of the underlying aluminum film. This is seen both in the increase of the signal from oxygen and in the chemical shift in the Al 2s electron emission peak toward higher binding energy as the surface of the metal oxidizes to Al^{+3}. The extent of oxide growth can be modeled from the relative area of each peak once they are corrected for the attenuation through MgF_2 layer. We showed the figure of merit used to choose the Lorentzian and Gaussian character for fitting the area of Al_2O_3 and Al peaks, and with this standard we showed that amount of oxidation increases with the logarithmic of time, by plotting the Al_2O_3/Al ratios.

Both XPS and SE allow the growth of the aluminum oxide to be tracked and quantified. Based on graphs of oxidation as a function of time, we produce a emperical formula: thickness= k*log(t) +b, which fits the measured time-dependent aluminum oxide thickness on aluminum surfaces protected by MgF_2. k is a factor that depends only on MgF_2 thickness, and decreases with increasing MgF_2 thickness. Values for k for various thicknesses are presented. These differ slightly between SE and XPS data. This study also contributes to the use of SE and XPS as analytical techniques generally. In

Downloaded From: https://www.spiedigitallibrary.org/conference-proceedings-of-spie on 14 Sep 2019
Terms of Use: https://www.spiedigitallibrary.org/terms-of-use

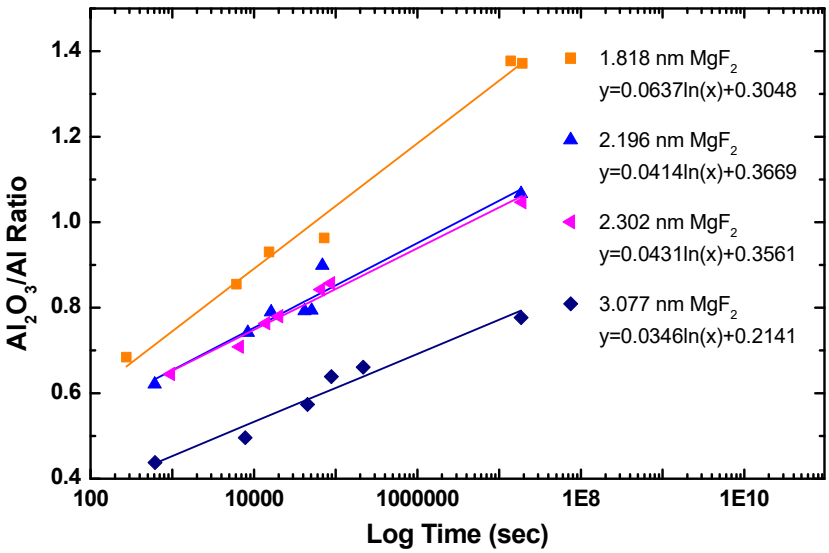


Figure 7 Graphical representation of Al_2O_3/Al Ratio Changes over 8-month time-period

their differing attenuation depths, this XPS study confirms the porosity of room temperature deposited ultrathin films and indicates that porosity decreases with increasing thickness. We also show that for each SE sample, the because the optical constants of ultrathin metals films depend strongly on deposition conditions and their thickness, the optical constants for Al, as well as the Al and Al_2O_3 thicknesses, need to be individually fit. Similarly, as another first, we show how dynamic SE data track oxide growth over a period of several hours after the evaporated Al + MgF_2 bilayer is first exposed to the air. In dynamic SE, measurements are made every few seconds.

The SE and techniques developed and presented here may be generally applicable for films protected by thicker fluoride layers and/or enhanced fluorides. Enhanced means films deposited at elevated temperature. These techniques may allow for extrapolation of barrier-layer effectiveness for room-temperature deposited MgF_2 on Al to thicker fluoride films and point the way to producing shortcut methods for identifying which films that could qualify for further study. However, it should be noted that the Al in the films suitable for these ellipsometric studies are a factor of 3-4 times too thin for standard telescope mirrors.

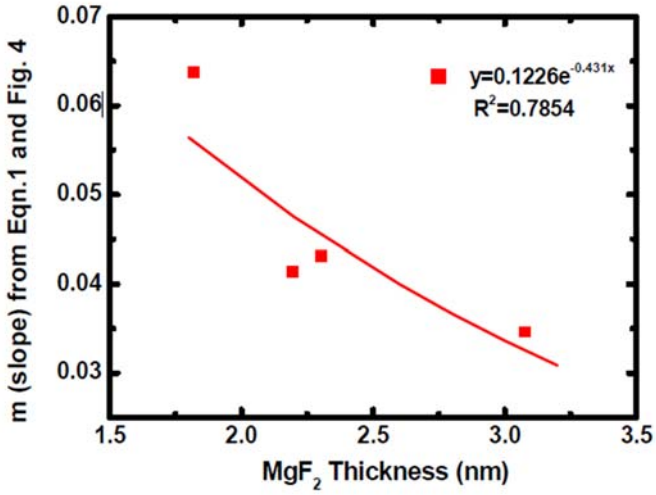


Figure 8. In large measure, the fit to these values here should be considered a guide to the eye.

Downloaded From: https://www.spiedigitallibrary.org/conference-proceedings-of-spie on 14 Sep 2019
Terms of Use: https://www.spiedigitallibrary.org/terms-of-use

ACKNOWLEDGMENTS

The authors gratefully thank and acknowledge the Utah NASA Space Grant Consortium under a NASA award-#NNX15AI24H to Utah Space Grant Consortium for funding a portion of Brian Johnson's research time and for supporting the project generally. We thankfully acknowledge John E. Ellsworth, Department of Physics and Astronomy, Brigham Young University for his help with vacuum systems and BYU's College of Physical and Mathematical Sciences for student support.

REFERENCES

[1] Bertram, R., Martchek, K. J. and Rombach, G., "Supplementary material for: Material flow analysis in the aluminum industry," J. Ind. Ecol. **13**(5), 650–654 (2009).
[2] Das, S. . Y. W., "Trends in the global aluminum fabrication industry," JOM **59**(2), 83–87 (2007).
[3] Skillingberg, M.; Green, J., "Aluminum applications in the rail industry," Light Met. Age-Chicago **65**(5), 8 (2007).
[4] Hass, G., Hunter, W. R. and Tousey, R., "Reflectance of evaporated aluminum in the vacuum ultraviolet," J. Opt. Soc. Am. **46**(5), 369 (1956).
[5] Hass, G. and Tousey, R., "Reflecting Coatings for the Extreme Ultraviolet*," J. Opt. Soc. Am. **49**(6), 593 (1959).
[6] Bridou, F., Cuniot-Ponsard, M., Desvignes, J.-M., Maksimovic, I. and Lemaire, P., "VUV mirrors for the (80-120 nm) spectral range," Adv. Opt. Thin Film. **5250**, C. Amra, N. Kaiser, and H. A. Macleod, Eds., 627–637 (2004).
[7] Brune, H., Wintterlin, J., Behm, R. J. and Ertl, G., "Surface migration of hot adatoms in the course of dissociative chemisorption of oxygen on Al(111)," Phys. Rev. Lett. **68**(5), 624–626 (1992).
[8] Do, T.; McIntyre, N.; Harshman, R; Lundy, M.; Splinter, S., "Application of parallel factor analysis and x-ray photoelectron spectroscopy to the initial stages in oxidation of aluminium. I. The Al 2p photoelectron line," Surf. interface Anal. **27**(7), 618–628 (1999).
[9] Trost, J.; Brune, H.; Wintterlin, J.; Behm, R. . E. G., "Interaction of oxygen with Al (111) at elevated temperatures," The Journal of chemical physics," J. Chem. Phys. **108**(4), 1740–1747 (1998).
[10] Zhukovskii, Y. F.; Jacobs, P. . C. M., "On the mechanism of the interaction between oxygen and close-packed single-crystal aluminum surfaces," J. Phys. Chem. Solids **64**(8), 1317–1331 (2003).
[11] Do, T.; Splinter, S.; Chen, C. ; McIntyre, N., "The oxidation kinetics of Mg and Al surfaces studied by AES and Values of m determined from Equation 1 and Figure 4. XPS," Surf. Sci. **387**(1–3), 192–198 (1997).
[12] Fernández-Perea, M., Larruquert, J. I., Aznárez, J. A., Pons, A. and Méndez, J. A., "Vacuum ultraviolet coatings of Al protected with MgF2 prepared both by ion-beam sputtering and by evaporation," Appl. Opt. **46**(22), 4871–4878 (2007).
[13] Lazić, I. and Thijsse, B. J., "An improved molecular dynamics potential for the Al–O system," Comput. Mater. Sci. **53**(1), 483–492 (2012).
[14] Madaan, N., Kanyal, S. S., Jensen, D. S., Vail, M. A., Dadson, A. E., Engelhard, M. H., Samha, H. and Linford, M. R., "Al2O3 e-Beam Evaporated onto Silicon (100)/SiO2, by XPS," Surf. Sci. Spectra **20**(1), 43–48 (2013).
[15] S. Kanyal, S., Jensen, D. S., Zhu, Z. and Linford, M. R., "Al2O3 e-beam evaporated onto silicon (100)/SiO2 by ToF-SIMS," Surf. Sci. Spectra **22**(2), 7–13 (2015).
[16] Sherwood, P. M. A., "Curve fitting in surface analysis and the effect of background inclusion in the fitting process," J. Vac. Sci. Technol. A **14**(3), 1424–1432 (1996).
[17] Allred, D. D., Turley, R. S., Thomas, S., Willett, S., Perry, S. B. and Greenburg, M. J., "Progress towards adding EUV reflectance to broadband Al mirrors for space-based observatories," Proc. SPIE **10398**, H. A. MacEwen and J. B. Breckinridge, Eds., 34, SPIE (2017).
[18] Marcos, L. V. R. De, Larruquert, J. I., Méndez, J. A., Gutiérrez-Luna, N., Espinosa-Yáñez, L., Honrado-Benítez, C., Chavero-Royán, J. and Perea-Abarca, B., "Optimization of MgF2-deposition temperature for far UV Al mirrors," Opt. Express **26**(7), 9363–9372 (2018).
[19] Fateh, B., Brooks, G. A., Rhamdhani, M. A., Taylor, J. A., Davis, J. and Lowe, M., "Study of Early Stage Interaction of Oxygen with Al; Methods, Challenges and Difficulties," [Light Metals 2011], S. J. Lindsay, Ed., Springer International Publishing, Cham, 725–730 (2016).

Downloaded From: https://www.spiedigitallibrary.org/conference-proceedings-of-spie on 14 Sep 2019
Terms of Use: https://www.spiedigitallibrary.org/terms-of-use

[20] Lousada, C. M. and Korzhavyi, P. A., "First stages of oxide growth on Al(1 1 0) and core-level shifts from density functional theory calculations," Appl. Surf. Sci. **441**, 174–186 (2018).
[21] Wilbrandt, S., Stenzel, O., Nakamura, H., Wulff-Molder, D., Duparré, A. and Kaiser, N., "Protected and enhanced aluminum mirrors for the VUV," Appl. Opt. **53**(4), A125--A130 (2014).
[22] Bolcar, M. R., Balasubramanian, K., Crooke, J., Feinberg, L., Quijada, M., Rauscher, B. J., Redding, D., Rioux, N., Shaklan, S., Stahl, H. P., Stahle, C. M. and Thronson, H., "Technology gap assessment for a future large-aperture ultraviolet-optical-infrared space telescope," J. Astron. Telesc. Instruments, Syst. **2**(4), 41209 (2016).
[23] Balasubramanian, K., Hennessy, J., Raouf, N., Nikzaa, S., Ayala, M., Shaklan, S., Scowen, P., Hoyo, J. Del, Quijada, M. and Howard A. MacEwen, J. B. B., "Aluminum Mirror Coatings for UVOIR Telescope Optics including the Far UV," [UV/Optical/IR Space Telescopes and Instruments: Innovative Technologies and Concepts VII: Proc. of SPIE Vol. 9602], SPIE, Bellingham,, WA, 96020I-1–9 (2015).
[24] Hennessy, J., Balasubramanian, K., Moore, C. S., Jewell, A. D., Nikzad, S., France, K. and Quijada, M., "Performance and prospects of far ultraviolet aluminum mirrors protected by atomic layer deposition," J. Astron. Telesc. Instru. Syst. **2**(4) (2016).
[25] Johnson, B. I.; Avval, T. G.; Hodges, G.; Membreno, K.; Carver, V.; Allred, D. D.; Linford, M. R., "Oxidation of Aluminum Protected by Wide Band Gap MgF2 Layers as Followed by X-ray Photoelectron Spectroscopy," TechCon 2019 62nd Annu. SVC Tech. Conf., SVC. NM USA, Long Beach Convention Center, Ca, (2019).
[26] Johnson, B. I.; Avval, T. G.; Hodges, G.; Membreno, K.; Allred, D. D.; Linford, M. R., "Real- Time Monitoring of Aluminum Oxidation Through Wide Band Gap MgF2 Layers for Protection of Space Mirrors," 2019 25th Annu. Fellowsh. Symp., Utah NASA Space Grant Consortium., Brigham Young University, Provo, UT USA (2019).
[27] Hilfiker, J. N., Singh, N., Tiwald, T., Convey, D., Smith, S. M., Baker, J. H. and Tompkins, H. G., "Survey of methods to characterize thin absorbing films with Spectroscopic Ellipsometry," Thin Solid Films **516**(22), 7979–7989 (2008).
[28] Cumpson, P. J. and Seah, M. P., "Elastic Scattering Corrections in AES and XPS. II. Estimating Attenuation Lengths and Conditions Required for their Valid Use in Overlayer/Substrate Experiments," Surf. Interface Anal. **25**(6), 430–446 (1997).
[29] Cumpson, P. J., "The Thickogram: a method for easy film thickness measurement in XPS," Surf. Interface Anal. **29**(6), 403–406 (2000).
[30] Baba, K., Shiraishi, K., Obi, K., Kataoka, T. and Kawakami, S., "Optical properties of very thin metal films for laminated polarizers," Appl. Opt. **27**(12), 2554–2560 (1988).
[31] Tompkins, H. G., Tasic, S., Baker, J. and Convey, D., "Spectroscopic ellipsometry measurements of thin metal films," Surf. Interface Anal. **29**(3), 179–187 (2000).
[32] Wyatt, D. M., Gray, R. C., Carver, J. C., Hercules, D. M. and Masters, L. W., "Studies of Polymeric Bond Failure on Aluminum Surfaces by X-ray Photoelectron Spectroscopy (ESCA)," Appl. Spectrosc. **28**(5), 439–445 (1974).
[33] Jain, V., Biesinger, M. C. and Linford, M. R., "The Gaussian-Lorentzian Sum, Product, and Convolution (Voigt) functions in the context of peak fitting X-ray photoelectron spectroscopy (XPS) narrow scans," Appl. Surf. Sci. **447**, 548–553 (2018).
[34] Shah, D., Patel, D. I., Roychowdhury, T., Rayner, G. B., O'Toole, N., Baer, D. R. and Linford, M. R., "Tutorial on interpreting x-ray photoelectron spectroscopy survey spectra: Questions and answers on spectra from the atomic layer deposition of Al2O3 on silicon," J. Vac. Sci. Technol. B **36**(6), 62902 (2018).
[35] Rotole, J. A. and Sherwood, P. M. A., "Gamma-Alumina (γ-Al2O3) by XPS," Surf. Sci. Spectra **5**(1), 18–24 (1998).
[36] Rotole, J. A. and Sherwood, P. M. A., "Corrundum (α-Al2O3) by XPS," Surf. Sci. Spectra **5**(1), 11–17 (1998).
[37] Strohmeier, B. R., "Gamma-Alumina (γ-Al2O3) by XPS," Surf. Sci. Spectra **3**(2), 135–140 (1994).

Downloaded From: https://www.spiedigitallibrary.org/conference-proceedings-of-spie on 14 Sep 2019
Terms of Use: https://www.spiedigitallibrary.org/terms-of-use